Vol. 45 (2014) ACTA PHYSICA POLONICA B No 7

HIGGS RESULTS FROM THE ATLAS EXPERIMENT (STANDARD MODEL AND BEYOND)*

Camila Rangel Smith

Department of Physics and Astronomy, Uppsala University
Box 516, 751 20 Uppsala, Sweden

(Received April 29, 2014)

The discovery of a new particle consistent with the Standard Model-like Higgs boson, with a mass of about 125 GeV, was announced by the ATLAS and CMS experiments on the 4th July, 2012. After the discovery, the properties of this new particle have been studied with high precision measurements of its mass, spin and couplings in all the accessible decay channels. In this paper, recent results from the ATLAS experiment are presented, including: $H \to \gamma\gamma$, $H \to ZZ^{(*)} \to 4l$, $H \to WW^{(*)} \to l\nu l\nu$, $H \to \tau\tau$, $H \to Z\gamma$, $H \to \mu\mu$ $VH \to b\bar{b}$, $VH \to WW^{(*)}$, $ttH \to \gamma\gamma$ channels. Furthermore, searches for beyond the standard model Higgs bosons are briefly reviewed.

DOI:10.5506/APhysPolB.45.1581
PACS numbers: 14.80.Bn, 14.80.Ec, 14.80.Fd

1. Introduction: Higgs boson physics

In the Standard Model (SM) [1–4], the Higgs boson couples preferentially to heavy particles, such as the Z boson, the W boson, and the top quark. Thus, the four main Higgs production modes in proton–proton collisions are:

- The dominant gluon–gluon fusion (ggF), where the Higgs boson couples indirectly to gluons via a triangular loop of quarks dominated by the top.
- The vector-boson fusion (VBF), in which the Higgs boson is produced by the fusion of two weak vector bosons radiated from quarks. The two recoiled quarks fragment into two forward jets with no QCD activity in between. The rapidity-gap signature can be used to suppress the QCD background.

* Presented at the Cracow Epiphany Conference on the Physics at the LHC, Kraków, Poland, January 8–10, 2014.

- The associated production with vector bosons (WH or ZH) is called Higgsstrahlung. It is an interesting mode to study couplings to the vector bosons.

- The Higgs production in association with top pairs (ttH) is the mode with the smallest cross section contributing to the LHC Higgs production. Nevertheless, it is an important process to measure the Yukawa coupling between the Higgs and the top quark.

The partial decay width of the Higgs boson depends on the mass of the decay products. In ATLAS a large number of exclusive decays of the Higgs boson are studied to determine the nature of this new particle. The most relevant channels are described in the next sections.

2. The $H \to \gamma\gamma$ channel

The di-photon channel was the first to observe the Higgs boson [5]. The analysis strategy is based on the di-photon invariant mass ($m_{\gamma\gamma}$) as a main discriminant variable, built by a photon pair with well measured energies and directions. For the search, the $m_{\gamma\gamma}$ range is scanned with the objective of finding a resonance peak, over a large QCD combinatorial background.

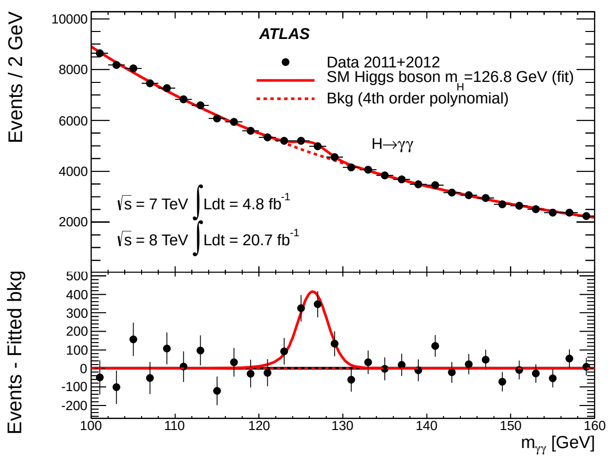

Fig. 1. Invariant mass distribution of di-photon candidates for the combined 7 TeV and 8 TeV data samples. The result of a fit to the data of the sum of a signal component fixed to an hypothesised Higgs mass of 126.8 GeV and a background component described by a fourth-order Bernstein polynomial is superimposed. The bottom inset displays the residuals of the data with respect to the fitted background component [5].

The background is composed of pairs of photons, associated production of photons with jets, and processes with several jets in the final state. To increase the analysis sensitivity, the events are separated into different categories with different mass resolutions and signal to background ratios. An extended unbinned maximum-likelihood fit is performed simultaneously to all categories to extract the signal and background event yields and determine the significance of the signal.

The analysis uses the complete dataset of the first LHC run of corresponding to an integrated luminosity of 20.7 fb^{-1} recorded at $\sqrt{s} = 8$ TeV and 4.7 fb^{-1} at $\sqrt{s} = 7$ TeV. In figure 1, the inclusive invariant mass distribution of the di-photon candidates is shown, overlaid with the signal-plus-background fit. The largest local signal significance in the combined data sample is found to be 7.4σ at a mass (m_H) of 126.5 GeV, where the expected significance is 4.1σ.

3. The $H \to ZZ^{(*)} \to 4l$ channel

Events are required to have two pairs of same-flavour, opposite charge, isolated leptons: $4e$, $2e2\mu$, $2\mu 2e$, 4μ. The largest background comes from di-boson $ZZ^{(*)}$ production. Important contributions arise also from Z+jets and $t\bar{t}$ production.

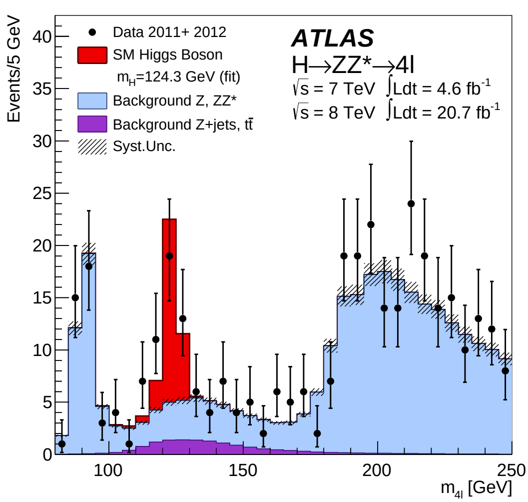

Fig. 2. The distribution of the four-lepton invariant mass, for the selected candidates in the data in the $H \to ZZ^{(*)} \to 4l$ channel. The estimated background, as well as the expected SM Higgs boson signal for $m_H = 124.3$ GeV, are also shown [5].

The mass reconstruction uses a constrained fit to the Z mass to improve the resolution, and the final state radiation (FSR) is included in the reconstruction of the leading Z decaying into muons. Similar to the $H \to \gamma\gamma$ channel, events are categorised separating candidate events into ggF-like, VBF- and VH-like events.

The analysis uses a sample with an integrated luminosity of 20.7 fb^{-1} recorded at $\sqrt{s} = 8$ TeV and 4.7 fb^{-1} at $\sqrt{s} = 7$ TeV. The reconstructed four-lepton mass spectrum of the inclusive analysis is shown in figure 2. A deviation from the background-only expectation is observed at a mass of 124.3 GeV, with a significance of 6.6σ for the combined 7 TeV and 8 TeV data (4.4σ expected). This result establishes a discovery-level signal in this channel alone [5].

4. The $H \to WW^{(*)} \to l\nu l\nu$ channel

The $H \to WW^{(*)} \to l\nu l\nu$ channel rate is large, but has a limited mass resolution due to the presence of two neutrinos in the final state. Events are required to have two opposite-charge leptons and a large missing energy from the neutrinos. The dominant SM backgrounds are $WW^{(*)}$, $t\bar{t}$ and Wt.

The events are categorised by jet multiplicity ($N_{\rm jets}$), which allows control of the background from top quarks (containing b-quark jets), as well as

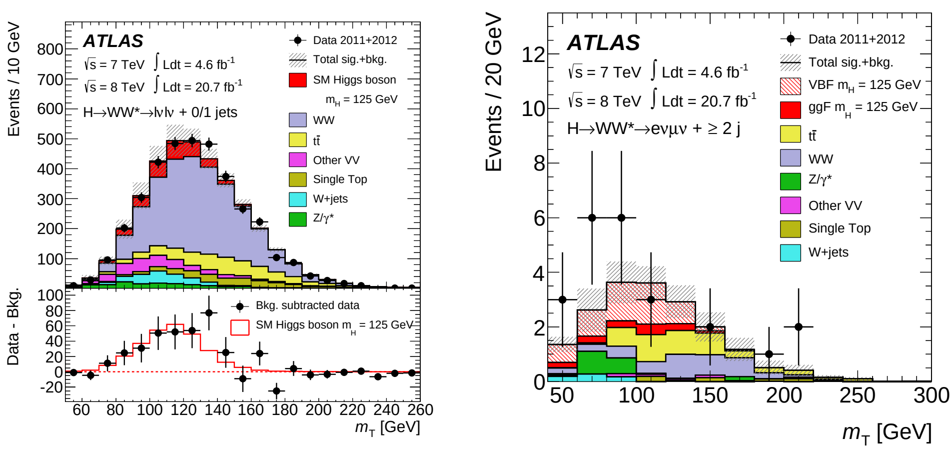

Fig. 3. Transverse mass distributions for events passing the full selection of the $H \to WW^{(*)} \to l\nu l\nu$ analysis: Left is summed over all lepton flavour combinations (electrons and muons) for final states with $N_{\rm jet} \leq 1$; on the right different-flavour final states with $N_{\rm jet} \geq 2$. The hatched area represents the total uncertainty on the sum of the signal and background yields from statistical, experimental, and theoretical sources [5].

the extraction of the signal strengths (μ defined as the ratio of the observed number of signal events to the expected in the SM) for the ggF and VBF production processes.

The transverse mass distributions for $N_{\rm jet} \leq 1$ and $N_{\rm jet} \geq 2$ final states are shown in figure 3 using a sample corresponding to the integrated luminosity of 20.7 fb^{-1} at $\sqrt{s} = 8$ TeV and 4.7 fb^{-1} at $\sqrt{s} = 7$ TeV. At $m_H = 125.5$ GeV, an excess of events over the background-only hypothesis corresponds to both observed in data and expected from simulation significance of 3.8σ for the SM Higgs boson [5], as shown in figure 4.

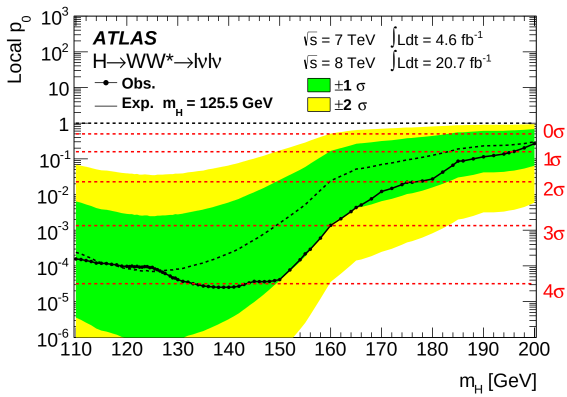

Fig. 4. The expected and observed local p_0 values as a function of m_H for the $H \to WW^{(*)} \to l\nu l\nu$ analysis of the combined 7 TeV and 8 TeV data. The grey/green (light grey/yellow) band indicates the $\pm1\sigma$ ($\pm2\sigma$) uncertainty on the expected p_0 curve [5].

5. The $H \to \tau\tau$ channel

The search is performed in all the τ decay combinations: $\tau_{\rm lep}$–$\tau_{\rm lep}$, $\tau_{\rm lep}$–$\tau_{\rm had}$ and $\tau_{\rm had}$–$\tau_{\rm had}$, using 20.7 fb^{-1} of data recorded at $\sqrt{s} = 8$ TeV. The dominating background is $Z \to \tau\tau$ (irreducible), followed by the reducible $Z(ee/\mu\mu)$+jets, W+jets, top, multi-jets and di-bosons. Each channel is affected differently by these backgrounds, therefore, the event selections are optimised separately.

Two analysis categories are defined in an exclusive way: VBF, with the presence of two jets with a large pseudo-rapidity separation and boosted, which is targeted at events with a boosted Higgs boson from ggF (Higgs $p_{\rm T} > 100$ GeV). The analysis strategy is based on a Boosted Decision Tree (BDT) used in each category to extract the Higgs signal from the large backgrounds.

A deviation from the background-only hypothesis is found with an observed (expected) significance of 4.1 (3.2) standard deviations, and a measured signal strength of $\mu = 1.4^{+0.5}_{-0.4}$. The compatibility of this excess of events above background predictions, with the SM Higgs boson at $m_H =$ 125 GeV is visualised with a weighted distribution of events as a function of $m_{\tau\tau}^{\mathrm{MMC}}$ (MMC stands for Missing Mass Calculator) [6], shown in figure 5.

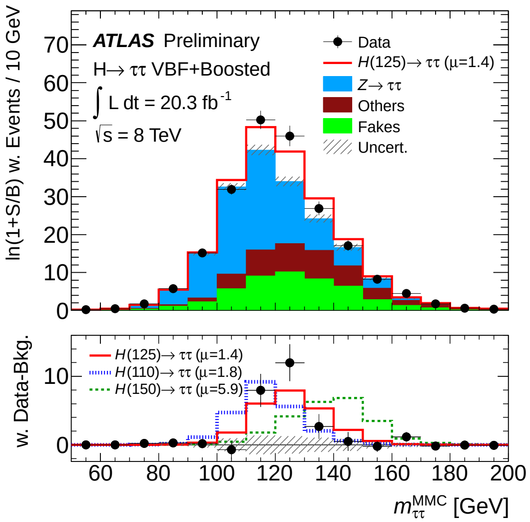

Fig. 5. Distribution for $m_{\tau\tau}^{\mathrm{MMC}}$ where events are weighted by $\ln(1 + S/B)$ for all channels. These weights are determined by the signal and background predictions for each BDT bin. The bottom panel shows the difference between weighted data events and weighted background events (black points), compared to the weighted signal yields. The background predictions are obtained from the global fit with the $m_H = 125$ GeV signal hypothesis ($\mu = 1.4$). The $m_H = 125$ GeV signal is plotted with a solid/red line with the signal strengths set to their best fit values [6].

6. Higgs properties measurements

The individual channels described in the previous sections are combined to extract information about the Higgs boson mass, production properties and couplings. Details of the statistical methods for the combination are found in [5]. A short summary of the results is presented in the following.

6.1. Mass and signal strength

The two channels with the best mass resolution are used for the mass determination: $H \to \gamma\gamma$ and $H \to ZZ^{(*)} \to 4l$. In the two cases, $m_H =$ $126.8 \pm 0.2(\mathrm{stat.}) \pm 0.7(\mathrm{sys.})$ GeV and $m_H = 124.3^{+0.6}_{-0.5}(\mathrm{stat.})^{+0.5}_{-0.3}(\mathrm{sys.})$ GeV are obtained from fits to the mass spectra.

The combined mass is measured to be

$$m_H = 125.5 \pm 0.2(\text{stat.})^{+0.5}_{-0.6}(\text{sys.})\ \text{GeV}\,, \tag{1}$$

where the main sources of systematic uncertainty are the photon and lepton energy and momentum scale.

The Higgs boson production strength μ is measured from a fit to the data using the profile likelihood ratio for a fixed mass hypothesis corresponding to the measured combined value $m_H = 125.5$ GeV.

The signal production strength normalised to the SM expectation, obtained by combining the $H \to \gamma\gamma$, $H \to ZZ^{(*)} \to 4l$ and $H \to WW^{(*)}$ channels, is

$$\mu = 1.33 \pm 0.14(\text{stat.}) \pm 0.15(\text{sys.})\,, \tag{2}$$

where the systematic uncertainty contributions from the theoretical uncertainty on the signal cross section and experimental sources are of similar magnitude. The summary of signal strengths, μ, measured in the main three channels and respective analysis categories are shown in figure 6.

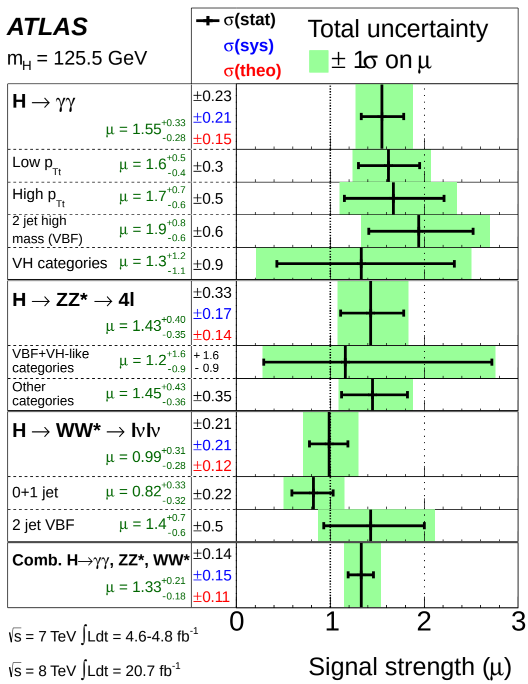

Fig. 6. The measured production strengths for a Higgs boson of mass $m_H = 125.5$ GeV, normalised to the SM expectations, for di-boson final states and their combination. Results are also given for the main categories of each analysis [5].

6.2. Coupling measurements

The measurements of couplings are implemented using a leading-order tree-level motivated framework. This framework is based on the assumption that the width of the Higgs boson is narrow and it is possible to use the zero width approximation. Hence the predicted rate for a given channel can be related to the production cross-section, and the partial and total Higgs boson decay widths in the following way

$$\sigma_x \mathrm{BR}\,(x \to H \to ff) = \frac{\sigma_x \Gamma_{ff}}{\Gamma_H}\,, \tag{3}$$

where σ_x is the production cross-section through the initial state x, BR and Γ_{ff} are the branching ratio and partial decay width into the final state ff, respectively, and Γ_H the total width of the Higgs boson.

In order to test the Higgs couplings to fermions and bosons, one coupling scale factor is assigned for fermions, κ_F, and one for bosons, κ_V. The results of the fit to data for the three channels and their combination are shown in figure 7. Here, $\kappa_V > 0$ is assumed, considering that only the relative sign of κ_F and κ_V is physical. The two-dimensional compatibility of the SM prediction with the best-fit value is 12%.

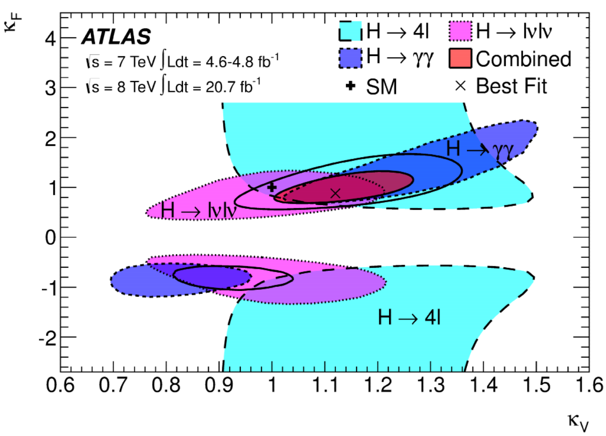

Fig. 7. Likelihood contours (68% C.L.) of the coupling scale factors κ_F and κ_V for fermions and bosons, as obtained from fits to the three individual channels and their combination (for the latter, the 95% C.L. contour is also shown). The best-fit result ($\times$) and the SM expectation ($+$) are also indicated [5].

The custodial symmetry is tested by measuring the ratio of couplings to the W and Z bosons normalised to the SM (λ_{WZ}). The fit to data yields $\lambda_{WZ} = 0.82 \pm 0.15$, giving the compatibility of the SM prediction with the best-fit value of 20%.

To test the existence of new heavy particles contributing to loop-induced processes, constraints on production and decay loops are extracted by introducing effective scale factors κ_g and κ_γ to parametrise the $gg \to H$ and $H \to \gamma\gamma$ loops. Figure 8 shows results of the measurements from a fit to data. The two-dimensional compatibility of the SM prediction with the best-fit value is 14%.

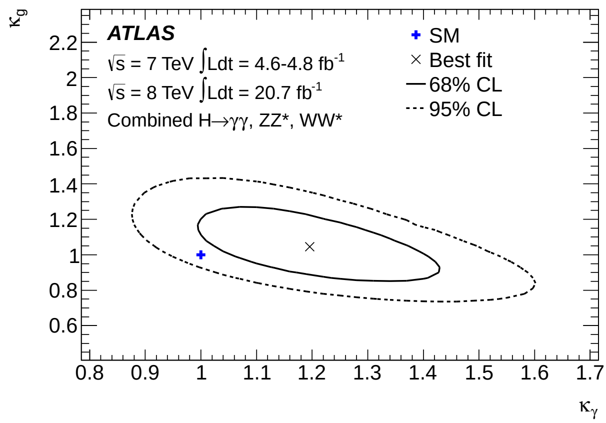

Fig. 8. Likelihood contours as a function of the effective coupling scale factors κ_F and κ_V, which are the ratios of the effective Higgs couplings to gluons and photons to the SM expectations [5].

6.3. Spin determination

Studies of the spin and parity quantum numbers of the Higgs boson are performed, using kinematic distributions for the $H \to \gamma\gamma$, $H \to ZZ^{(*)} \to 4l$ and $H \to WW^{(*)}$ decays modes. The data are compatible with the quantum numbers of the Higgs boson predicted by the Standard Model ($J^{\mathrm{P}} = 0^+$), whereas all alternative hypotheses studied, such as $J^{\mathrm{P}} = 0^-, 1^+, 1^-, 2^+$, are excluded at confidence levels above 97.8% [7], as shown in figure 9.

6.4. Differential cross sections measured in the $\gamma\gamma$ channel

The cross sections are measured using 20.3 fb^{-1} of data at $\sqrt{s} = 8$ TeV, in a dataset with a similar selection to the $H \to \gamma\gamma$ analysis for the fiducial range of $|\eta| < 2.37$ and with 105 GeV $< m_{\gamma\gamma} <$ 160 GeV. For each differential measurement, the dataset is divided in bins of different observables such as the transverse momentum $p_{\mathrm{T}\gamma\gamma}$ and rapidity $|y_{\gamma\gamma}|$ of the Higgs boson, the helicity angle $\cos\theta^*$ and the jet multiplicity.

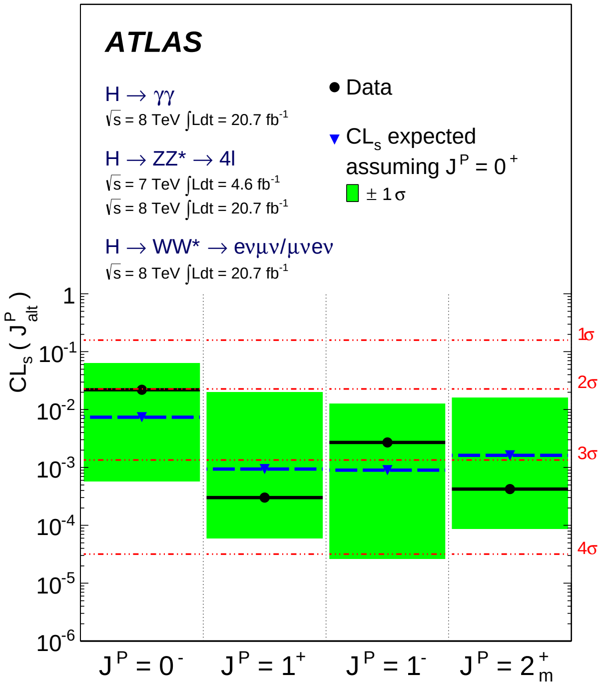

Fig. 9. Expected (blue triangles/dashed lines) and observed (black circles/solid lines) confidence level C.L.s for alternative spin-parity hypotheses assuming a 0+ signal. The grey/green band represents the 68% C.L.s ($J^{\rm P}_{\rm alt}$) expected exclusion range for a signal with assumed 0^+ [7].

For each observable and in every bin, the resonant signal yield is separated from backgrounds using signal plus background fits to the di-photon invariant mass spectrum. These yields are corrected for detector acceptance as well as resolution in the measured observable to determine the fiducial differential cross sections.

The unfolded differential cross sections for $p_{\gamma\gamma}$, $|y_{\gamma\gamma}|$, $\cos\theta^*$ and leading jet $p_{\rm T}$ are shown in figure 10. The measured differential cross sections are compared with various theoretical predictions. Within the experimental and theoretical uncertainties, no significant deviation from the SM expectation is observed [8].

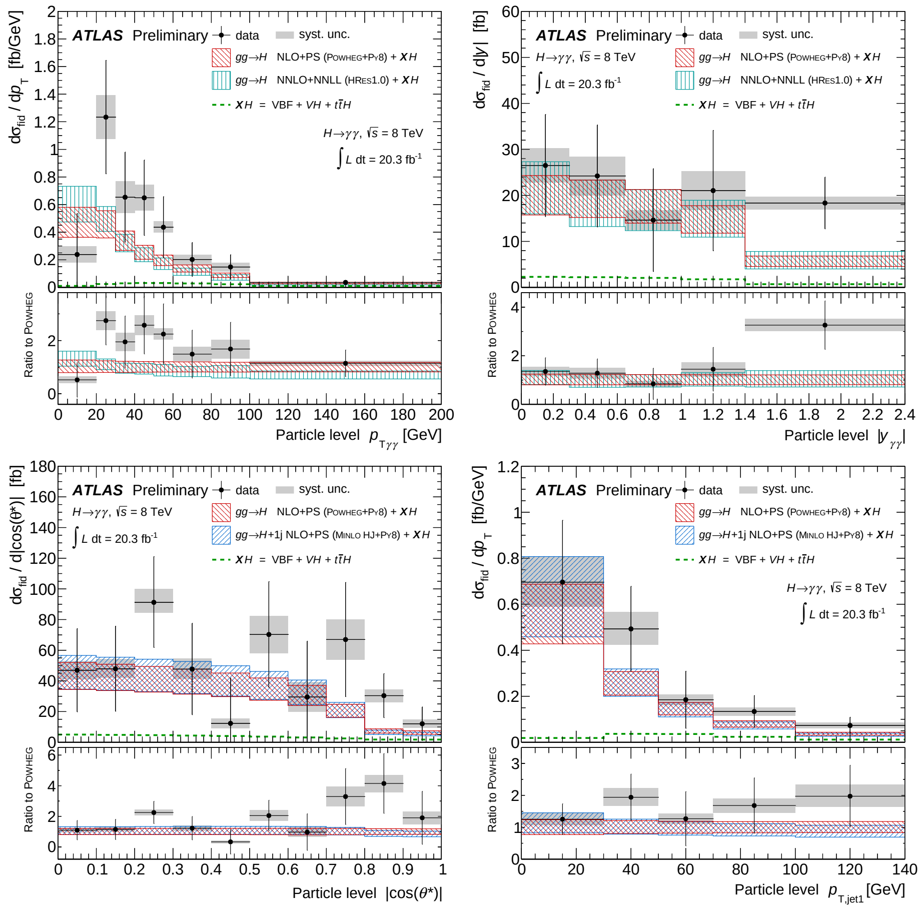

Fig. 10. Observed differential cross sections of the Higgs boson decaying into two isolated photons, for p_{T}, rapidity, $\cos\theta*$, and leading jet p_{T}. Systematic uncertainties are presented in grey, and the black bars represent the quadratic sum of statistical and systematic errors [8].

7. Rare production and decay modes

7.1. $H \to Z\gamma$

The search for the SM Higgs decaying into a $Z\gamma$ is performed using 20.7 fb^{-1} of recorded data at $\sqrt{s} = 8$ TeV and 4.6 fb^{-1} at $\sqrt{s} = 7$ TeV. No significant deviation from the SM prediction is observed and upper limits on the cross section of a Higgs boson with a mass between 120 and 150 GeV are derived. For a Higgs boson mass of 125 GeV, the expected and observed limits are 13.5 and 18.2 times the Standard Model, respectively [9].

7.2. $H \to \mu\mu$

The search in the $H \to \mu\mu$ channel is performed using 20.7 fb^{-1} of data at $\sqrt{s} = 8$ TeV. No evidence of a signal is observed and upper limits are set on the Higgs boson production as a function of the mass. The observed (expected) limit at the 95% C.L. for the Higgs boson with a mass of 125 GeV is 9.8 (8.2) times the SM prediction [10].

7.3. $pp \to (V)(H \to bb)$

A search for the $b\bar{b}$ decay of the SM Higgs boson in associated production with a W or Z boson is performed using 4.7 and 20.3 fb^{-1} of data at 7 and 8 TeV, respectively. No significant excess is observed above the expected SM backgrounds. For $m_H = 125$ GeV, a 95% C.L. upper limit of 1.4 times the SM expectation is set on the cross section times branching ratio [11].

7.4. $pp \to (tt)(H \to \gamma\gamma)$

A search for the ttH production mode is performed, using the leptonic and hadronic decay modes of the top quarks and the di-photon decay of the Higgs boson. The analysis uses 20.3 fb^{-1} of proton–proton collisions at $\sqrt{s} = 8$ TeV. No excess over the background prediction is observed and limits are set on the production. The observed (expected) 95% confidence level exclusion limits on the ttH production cross section for a Higgs boson with a mass of $m_H = 126.8$ GeV are 5.3 (6.4) times the predicted SM values [12].

7.5. $pp \to (V)(H \to WW^{(*)})$

A search for the VH associated production modes, with the subsequent decay $H \to WW^{(*)} \to l\nu l\nu$, is performed using 20.7 fb^{-1} of data at $\sqrt{s} = 8$ TeV and 4.7 fb^{-1} of data recorded at $\sqrt{s} = 7$ TeV. No significant excess is observed over the Standard Model expectations and limits at 95% C.L. on the cross section ratio to the SM prediction are set for 110 GeV $< m_H <$ 200 GeV. The observed (expected) limit for a Higgs boson of mass $m_H =$ 125 GeV is found to be 7.2 (3.6) times the SM cross section [13].

8. BSM Higgs searches

8.1. Search for a multi-Higgs-boson cascade in $W^+W^-b\bar{b}$ events

A search for new particles in an extension to the SM that includes a heavy Higgs boson (H_0), an intermediate charged Higgs-boson pair ($H^{\pm}$), and a light Higgs boson (h_0) with a mass of 125 GeV, is performed using 20.3 fb^{-1} of 8 TeV data. In the analysis, events involving the production of a single heavy neutral Higgs boson decaying to the charged Higgs boson and a W boson are searched, where the charged Higgs boson subsequently decays into a W boson and the lightest neutral Higgs boson decaying to $b\bar{b}$ pair. The data are found to be consistent with Standard Model predictions, and 95% confidence-level upper limits are set on the product of cross section and branching ratio [14], as shown in figure 11.

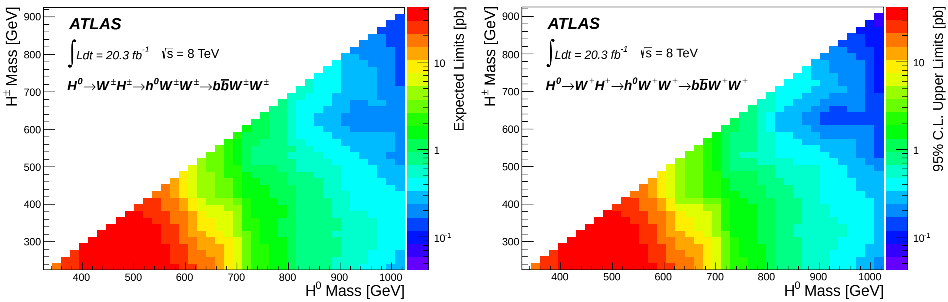

Fig. 11. The expected (left) and observed (right) 95% C.L. upper limits on the cross section for $gg \to H_0 \to WH^{\pm} \to WW^{(*)}h \to WW^{(*)}bb$ as a function of $m(H_0)$ and m($H^{\pm}$) [14].

8.2. *Search for $H^{\pm} \to \tau\nu$*

The search for $H^{\pm} \to \tau\nu$ with a hadronically decaying τ lepton in the final state uses 19.5 fb^{-1} of data recorded at $\sqrt{s} = 8$ TeV. No evidence for a charged Higgs boson is found and 95% C.L. limits on $B(t \to H^{\pm}b)$ are set for the mass range 90 GeV $< m(H^{\pm}) <$ 160 GeV, and for the mass range 180 GeV $< m(H^{\pm}) <$ 600 GeV, upper limits are set on the production cross section [15], both with the assumption that $B(H^{\pm} \to \tau\nu)$=1 (figures 12 and 13).

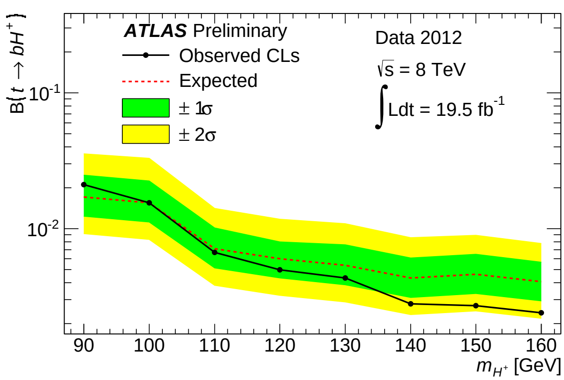

Fig. 12. The expected and observed 95% C.L. upper limits on $B(t \to H^{\pm}b)$ for a light charged Higgs boson, with the assumption that $B(H^{\pm} \to \tau\nu) = 1$ [15].

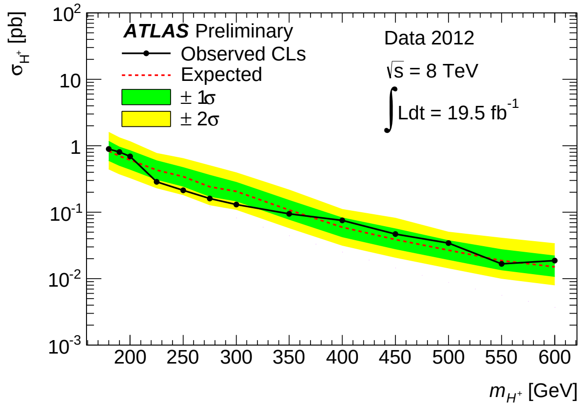

Fig. 13. The expected and observed 95% C.L. upper limits on the production cross-section for a heavy charged Higgs, with the assumption that $B(H^{\pm} \to \tau\nu) = 1$ [15].

9. Summary

After the discovery of the new boson, its properties are being measured using the full LHC Run I ATLAS data from the $H \to \gamma\gamma$, $H \to ZZ^{(*)} \to 4l$, $H \to WW^{(*)} \to l\nu l\nu$ decay channels. The combined mass measurement yields $m_H = 125.5 \pm 0.2(\text{stat.})^{+0.5}_{-0.6}(\text{sys.})$ GeV, the combined signal strength $\mu = 1.33 \pm 0.14(\text{stat.}) \pm 0.15(\text{sys.})$, and the spin/parity measurements favour spin 0^+, as predicted by the Standard Model.

The first and preliminary results on evidence for direct fermionic decay $H \to \tau\tau$ have been presented, where the deviation from the background-only hypothesis is found with an observed (expected) significance of 4.1 (3.2). Furthermore, various rare production decay modes and BSM Higgs models searches have been briefly discussed.

The ATLAS experiment is now preparing for the LHC Run II, where sensitivity for observation of rare SM Higgs production/decays should be achieved and more precise measurements will be performed to test and challenge the SM predictions.

REFERENCES

[1] S. Glashow, *Nucl. Phys.* **22**, 579 (1961).
[2] S. Weinberg, *Phys. Rev. Lett.* **19**, 1264 (1967).
[3] A. Salam, *Conf. Proc.* **C680519**, 367 (1968).
[4] G. 't Hooft, M. Veltman, *Nucl. Phys.* **B44**, 189 (1972).
[5] ATLAS Collaboration, *Phys. Lett.* **B726**, 88 (2013).

[6] ATLAS Collaboration, technical report ATLAS-CONF-2013-108, Nov 2013, `https://cds.cern.ch/record/1632191`

[7] ATLAS Collaboration, *Phys. Lett.* **B726**, 120 (2013).

[8] ATLAS Collaboration, technical report ATLAS-CONF-2013-072, Jul 2013, `https://cds.cern.ch/record/1562925`

[9] ATLAS Collaboration, technical report ATLAS-CONF-2013-009, Mar 2013, `https://cds.cern.ch/record/1523683`

[10] ATLAS Collaboration, technical report ATLAS-CONF-2013-010, Mar 2013, `https://cds.cern.ch/record/1523695`

[11] ATLAS Collaboration, technical report ATLAS-CONF-2013-079, Jul 2013, `https://cds.cern.ch/record/1563235`

[12] ATLAS Collaboration, technical report ATLAS-CONF-2013-080, Jul 2013, `https://cds.cern.ch/record/1564319`

[13] ATLAS Collaboration, technical report ATLAS-CONF-2013-075, Jul 2013, `https://cds.cern.ch/record/1562933`

[14] ATLAS Collaboration, *Phys. Rev.* **D89**, 032002 (2014).

[15] ATLAS Collaboration, technical report ATLAS-CONF-2013-090, Aug 2013, `https://cds.cern.ch/record/1595533`